

## Robotic-based laser ultrasonic non-destructive testing of 3D-printed continuous fiber reinforced flight control surface

Kyu-Jin Lee<sup>1</sup>, Jung-Ryul Lee<sup>2\*</sup>

Department of Aerospace Engineering, Korea Advanced Institute of Science and Technology, 291 Daehak-ro, Yuseong-gu, Daejeon 34141,

<sup>1</sup> pos2323@kaist.ac.kr, <sup>2\*</sup> leejrr@kaist.ac.kr

**Abstract:** The development of 3D printing technology using various materials has led to the emergence of printing technology utilizing carbon fiber, which suggests its potential application in the aerospace industry. The use of continuous carbon fiber for 3D printing can simplify the existing composite material manufacturing process, but research is needed on non-destructive visualization techniques to detect defects that may occur during the manufacturing process. In this paper, we propose a non-destructive testing system utilizing a 6-axis robotic arm and laser ultrasonic testing (LUT), along with a calculation method for inspection paths. The target of the inspection was the control surface of an aircraft, which was fabricated using a continuous fiber 3D printer. The control surface was fixed at the tip of the 6-axis robotic arm, and a full-area inspection was performed by controlling its position. By using the proposed inspection technique, we obtained a high signal-to-noise ratio from ultrasonic signals generated by the laser. The reliability of the proposed inspection technique was verified through analysis of the inspection results.

**Keywords:** Robotic scanning, Laser ultrasonic testing, Additive manufacturing, Carbon-fiber-reinforced polymers

### INTRODUCTION

3D printing technology has emerged as a remarkable innovation in the manufacturing industry. It enables the creation of various parts based on user-modeled 3D files and typically uses thermoplastic materials such as acrylonitrile butadiene styrene (ABS), polylactic acid (PLA), polyethylene terephthalate glycol (PETG), and Nylon [1, 2]. Among the various 3D printing techniques, material extrusion, which melts and extrudes materials, is mainly used [3]. However, those plastic materials have limitations in terms of their strength and weight, making it difficult to apply to the aerospace industry where high stiffness and strength are needed [1].

To combine the advantages of 3D printing technology and composite materials, 3D printing technology using continuous fiber filaments has emerged [4–6]. Similar to the composite production process of stacking ply sheets, continuous fibers are placed layer by layer during the printing process. Furthermore, users can place the fiber specifically in areas where reinforcement is needed. The properties of

composites made by continuous fiber 3D printing have been verified through various studies and suggest the potential for replacing traditional composite manufacturing processes [7].

The 3D printing technology using continuous fiber is recognized as a manufacturing technology suitable for small-scale and customized production. However, it has lower fiber volume fraction and production size limitations compared to the continuous fibers commonly used for composites, which makes it difficult to be used as the primary structure [8]. Therefore, to be applied in the aerospace industry, it can be used mainly in a secondary structure that has complex shapes and requires rapid supply. Alternative options need to be explored, and they can be highly applicable in the civilian aviation industry, such as the unmanned air mobility (UAM) industry.

Defects that occur in the manufacturing process of continuous fiber 3D printing include debonding and voids between extruded filaments [5, 8]. These occur mainly due to the behavior of high-stiffness continuous fibers or calibration errors that occur during long-term printing. These defects are directly related to the deterioration of the mechanical properties of the manufactured parts [9]. For composite parts made by continuous fiber 3D printers to be applied in practice, an assessment of the manufacturing suitability based on non-destructive testing is required. Common non-destructive testing methods for composite include micro-computed tomography (micro-CT), water squirt ultrasonic testing, and phased array ultrasonic testing (PAUT) [10–12]. However, their application is limited due to the vulnerability of composite materials to moisture and the shape or size constraints of the inspection targets. In contrast, laser ultrasonic testing (LUT) is suitable for integration with automated systems using robots, as they do not require separate ultrasonic transmission media or contact-type probes [13]. Therefore, this paper introduces a robot-based automated system using LUT and verifies its feasibility for detecting manufacturing defects in continuous fiber 3D-printed aircraft parts.

## METHODOLOGY

This section consists of four main headings. In the first heading, we introduce the aircraft control surface, which is the inspection target fabricated by a continuous fiber 3D printer. In the second heading, we qualitatively explain the principle of ultrasonic generation by a pulsed laser. In the third heading, we describe how the laser ultrasonic principle was applied to the system and explain the inspection techniques used. Finally, in the fourth section, we present an approach to calculating scan points.

### Fabrication of a flight control surface

The selected component for inspection was the control surface (aileron) of the unmanned air mobility wing. If the component is replaced with continuous fiber 3D printing instead of the traditional composite manufacturing method, significant reductions in fabrication time and cost can be achieved. Due to the maximum size limit that can be produced with continuous fiber 3D printing, the control surface was divided into three parts as shown in Figure 1. The selected part of the control surface was part 1, which is closer to the root section. Therefore, the height was set to 160 mm.

Figure 2 (a) shows an image taken during the 3D printing process. The stacking direction was arranged so that the cross-section of the control surface was parallel to the printer bed, taking into consideration the surface roughness and height resolution of the printer. The cross-section of the airfoil is presented in Figure 2 (b). Two loops of continuous carbon fiber filament were placed along the outer wall of the airfoil for external reinforcement. The interior was constructed using a triangular infill pattern with chopped carbon fiber filament. To verify the defect detection capability of the inspection system and the accuracy of the inspection path calculation, the control surface was imitated with an artificial defect. The artificial defect was a debonding between the chopped carbon fiber used to construct the outer wall of the control surface and the continuous carbon fiber used for reinforcement.

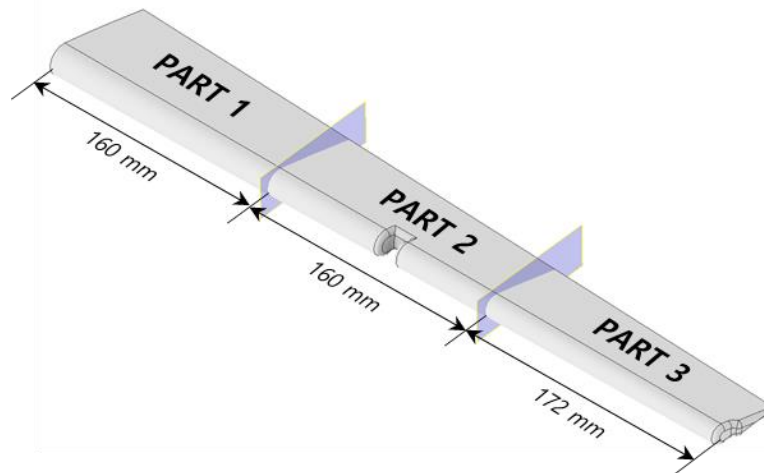


Figure 1: Segmented control surface of UAM.

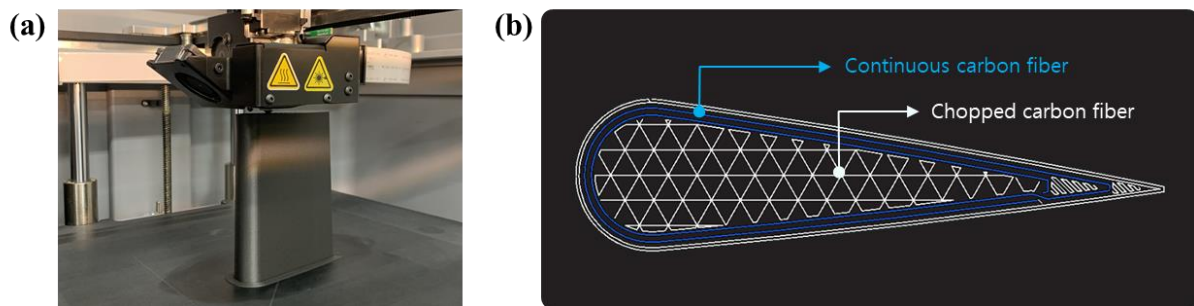


Figure 2: Fabrication of 3D-printed control surface: (a) image of the continuous fiber 3D printing process, (b) placement of carbon fiber filaments.

### Laser ultrasonic testing

The non-destructive testing technique used in this paper was LUT, which generates ultrasonic waves when a pulsed laser is irradiated onto a solid surface. Two lasers were used for ultrasonic generation and measurement. An excitation laser with a pulse width in the nanosecond range was used for generating ultrasonic in solid media. When the pulsed laser irradiates the solid surface, temporary energy absorption occurs at the surface layer, and thermoelastic waves are generated in the thermoelastic regime, without exceeding the damage threshold of the solid. The generated thermoelastic waves propagate in the form of ultrasonic waves with a broad frequency range [14].

Generally, contact sensors are used for measuring the generated ultrasonic signals such as piezoelectric sensors [15]. In this study, a laser Doppler vibrometer (LDV) was used for measurement. The LDV measures the waveform and amplitude of the generated ultrasonic wave using the Doppler shift phenomenon of the laser emitted from the sensor head. Therefore, generation and measurement are performed simultaneously, it can be used as a completely non-contact non-destructive testing technique.

### Robotic pulse-echo laser ultrasonic testing system

To measure high-quality ultrasonic signals using LDV, two constraints should be considered. The first is the distance between the surface of the target and the measurement beam. The measurement beam of LDV is aligned with the beam focus at the distance to be measured, so any variation in the measurement distance during the inspection process leads to a decrease in signal level, increasing the noise. The second constraint is that the measurement beam of LDV must be incident perpendicular to the surface of the target and reflected. If the angle between the inspection surface and the measurement beam changes during the inspection, it results in a decreased signal-to-noise ratio (SNR).

To address these limitations, we propose a robotic pulse-echo LUT system capable of inspecting curved structures over the entire surface. The robotic arm was a key component of the system, providing precise

manipulation and a wide range of motion for operation. The object being inspected was fixed at the end defined as the tool center point (TCP) of the robotic arm. By calculating the coordinates and quaternion of the TCP, the inspection path could be implemented, making it possible to apply the LUT for various curved shapes.

One of the inspection modes of LUT applied in the inspection system was the pulse-echo, which irradiates the excitation laser and LDV beam in the same direction [16]. The schematic diagram of the pulse-echo mode is shown in Figure 3. The ultrasonic wave generated at the surface can be divided into a direct wave and a back-wall echo, propagating in the thickness direction. If there is a defect or damage in the medium through which the ultrasonic wave propagates, the ultrasonic wave can not propagate due to the impedance change. This results in a difference in the back-wall echo signal. Therefore, by measuring the waveform or phase change of the back-wall echo during the inspection, defects can be visualized.

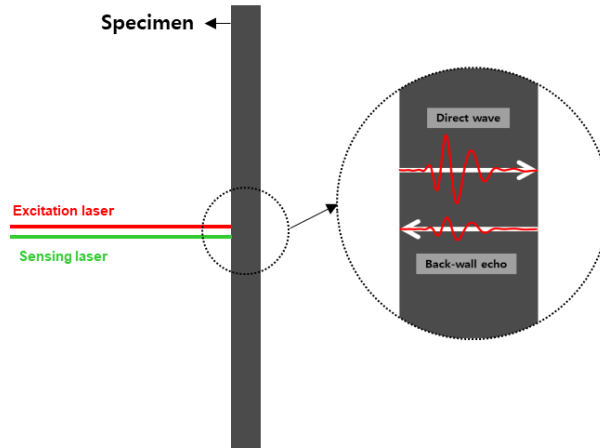


Figure 3: Schematic of pulse-echo mode.

#### Calculation of a scan point

The robotic pulse-echo laser ultrasonic testing system performs inspection by controlling the position of the control surface, which is attached to the robotic arm. Lasers remain fixed in place while the control surface is moved. To perform the inspection, the system calculates the cartesian coordinates, and the quaternion of the robotic arm's TCP to match the shape of the control surface. Information on the airfoil cross-section, as shown in Figure 4, was used to determine these coordinates. Figure 4 (a) displays the cartesian coordinates and quaternion at the  $n^{\text{th}}$  point representing the orientation of the frame with respect to the surface normal vector of the airfoil cross-section. By using equations (1) and (2), the quaternion  $\mathbf{q}_n$  at the  $n^{\text{th}}$  point is transformed into a rotation matrix  $\mathbf{R}$  that matches the  $\mathbf{q}_{tcp}$ . Figure 4 (b) illustrates the process of calculating the TCP coordinates. The rotated  $n^{\text{th}}$  point  $(x'_n, y'_n, z'_n)$  was symmetrically translated with respect to the TCP to obtain  $(x_s, y_s, z_s)$ , which was the final input value for the cartesian coordinates.

$$\mathbf{q}_n = [q_0, q_1, q_2, q_3] \quad (1)$$

$$\mathbf{R} = \begin{bmatrix} 2q_0^2 - 1 + 2q_1^2 & 2(q_1q_2 + q_0q_3) & 2(q_1q_3 - q_0q_2) \\ 2(q_1q_2 - q_0q_3) & 2q_0^2 - 1 + 2q_2^2 & 2(q_2q_3 + q_0q_1) \\ 2(q_1q_3 + q_0q_2) & 2(q_2q_3 - q_0q_1) & 2q_0^2 - 1 + 2q_3^2 \end{bmatrix} \quad (2)$$

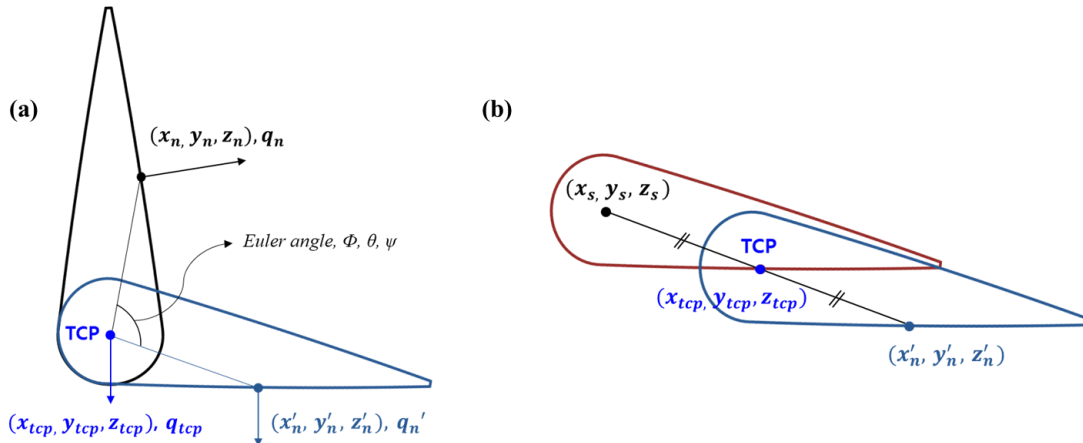


Figure 4: The airfoil cross-section of the control surface, (a) calculation of rotation, (b) calculation of translation.

## RESULTS

### The inspection result using an ultrasonic wave propagation imager (UWPI)

Using the described techniques in the Methodology section, we obtained the inspection results for the entire area of the control surface that was fabricated using continuous fiber 3D printing. The information for the lasers used for the inspection is provided in Table 1.

Table 1: Specifications of the lasers used for inspection.

<i>Excitation laser (Q-switched)</i>		<i>Laser Doppler vibrometer (LDV)</i>	
Wavelength	1064 nm	Wavelength	1550 nm
Laser medium	Nd:YAG	Dynamic range	200 mm/s/V
Pulse repetition frequency	240 Hz	Maximum frequency	3 MHz
Pulse energy	3.78 mJ	Laser power	< 10 mW

By acquiring the ultrasonic wave signals at each scan point, they can be placed in a 2D space that corresponds to the inspection area, resulting in an ultrasonic wave propagation imager (UWPI) that visualizes the propagated signals over time [17]. Figure 5 shows the UWPI results, visualization of a total of 1455 data points in the width direction and 960 data points in the height direction. Three images were obtained with a time interval of 0.2  $\mu\text{s}$ , and it can be observed that the gray color map changes in the image due to the amplitude variation of the signal. Since the control surface fabricated by continuous fiber 3D printing has intentionally induced defects, the difference in ultrasonic wave propagation images between the left and right sides can be observed in the inspection result.

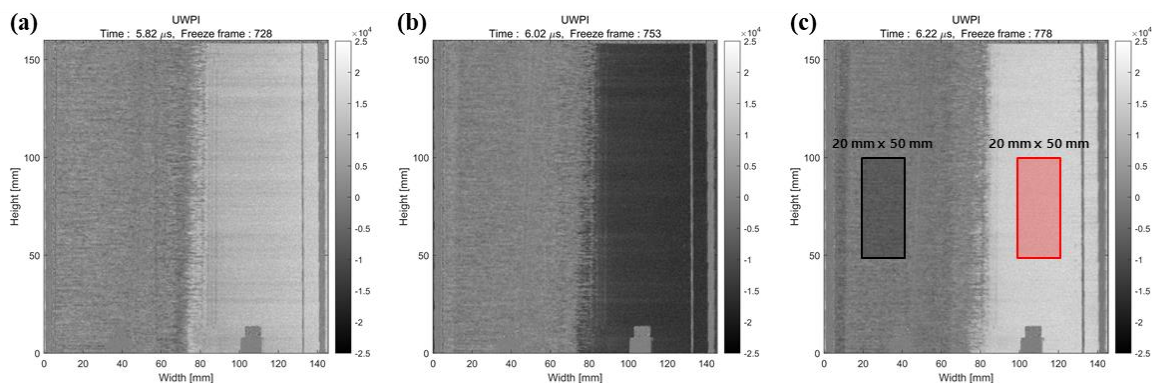


Figure 5: Inspection results of the control surface: (a) UWPI at 5.82  $\mu\text{s}$ , (b) UWPI at 6.02  $\mu\text{s}$ , (c) UWPI at 6.22  $\mu\text{s}$ .

### An analysis of ultrasonic signals

To perform a detailed analysis from the perspective of ultrasonic signals, two regions in the shape of a 20 mm x 50 mm box were selected as shown in Figure 5 (c). The comparison of averaged ultrasonic signals in each box is presented in Figure 6. From the averaged ultrasonic signals, it was confirmed that the direct wave generated by the initial laser pulse was the same. The difference was observed in the back-wall echo signal, which was caused by the thickness difference between the normal and defective regions. The thickness difference was the debonding between the continuous and chopped carbon fiber filaments, as presented in Figure 2 (b). In the region with a defect, the thickness decreases due to debonding, causing a decrease in the ultrasonic signal propagation distance, resulting in the overlap of the direct wave and back-wall echo signals. Therefore, in the suspected defective region, the signal shows a tendency to oscillate repeatedly.

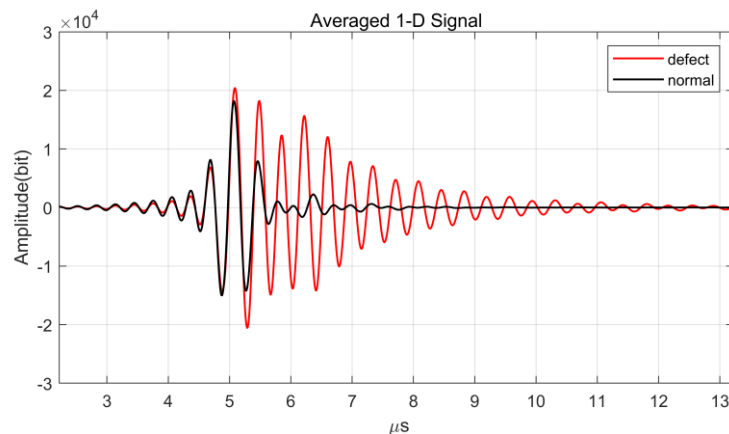


Figure 6: Comparison of averaged ultrasonic signals.

### The inspection result using a variable time window amplitude mapping (VTWAM)

To visualize the inspection results from the acquired ultrasonic signals data into a single image, we utilized variable time window amplitude mapping (VTWAM) [18]. The selected time window was from 6.10 to 6.80  $\mu\text{s}$ , where the back-wall echo signal difference occurred. The results are shown in Figure 7. The VTWAM results clearly distinguished between the normal and defective regions, where the blue area indicates the normal area and the red area indicates the defective area. By placing the inspection data in a 3D space using the shape information of the control surface, images shown in Figures 7 (b) and (c) could be obtained. Since those 3D plotted images have the same dimensions as the inspection target, we can intuitively identify the location of defects.

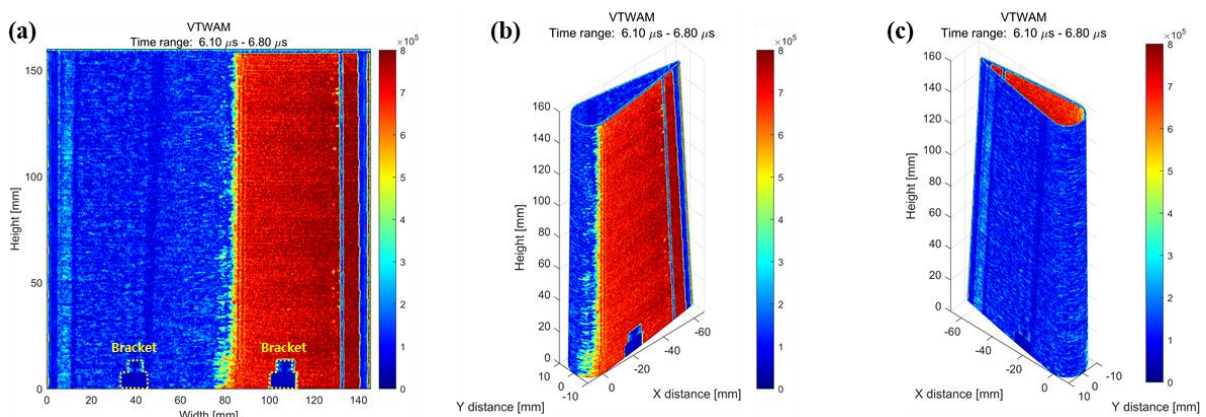


Figure 7: Post-processed results: (a) VTWAM result, (b) VTWAM result in 3D coordinates (right side view), (c) VTWAM result in 3D coordinates (left side view).

## CONCLUSION

This study presents a robotic pulse-echo laser ultrasonic testing technique that can be applied to aircraft components fabricated using continuous fiber 3D printing. The inspection target was fabricated using continuous and chopped carbon fiber filaments. To conduct the inspection, quaternion-based rotation transformation and coordinate transformation were used, and the validity of the calculated inspection points and paths was verified.

The inspection process involved acquiring ultrasonic signals, which were then placed in a 2D space to obtain the UWPI that visualized the propagated signals over time. To further analyze the inspection results, two regions were selected to compare the averaged ultrasonic signals. The difference in back-wall echo signal was caused by a thickness difference between normal and defective regions. The defective regions were characterized by a debonding between continuous and chopped carbon fiber filaments, which caused a decrease in thickness.

To visualize the inspection results in a single image, VTWAM was used. The VTWAM results clearly distinguished between normal and defective regions, and 3D plotted images were obtained using the shape information of the control surface. Overall, this study demonstrated the effectiveness of the robotic pulse-echo laser ultrasonic testing system for inspecting parts fabricated using continuous fiber 3D printing technology.

## ACKNOWLEDGEMENT

This study was supported by the Unmanned Vehicles Core Technology Research and Development Program through the National Research Foundation of Korea (NRF) and the Unmanned Vehicle Advanced Research Center (UVARC) funded by the Ministry of Science and Information and Communication Technology (ICT), Republic of Korea (NRF-2020M3C1C1A01084220). We also performed this study based on research which has been conducted as part of the KAIST-funded Global Singularity Research Program for 2023.

## REFERENCES

- [1] Jo, M. Y., Ryu, Y. J., Ko, J. H., & Yoon, J. S. (2012). Effects of compatibilizers on the mechanical properties of ABS/PLA composites. *Journal of Applied Polymer Science*, 125(SUPPL. 2). <https://doi.org/10.1002/app.36732>
- [2] Szykiedans, K., Credo, W., & Osiński, D. (2017). Selected Mechanical Properties of PETG 3-D Prints. *Procedia Engineering*, 177, 455–461. <https://doi.org/10.1016/j.proeng.2017.02.245>
- [3] Brenken, B., Barocio, E., Favaloro, A., Kunc, V., & Pipes, R. B. (2018). Fused filament fabrication of fiber-reinforced polymers: A review. In *Additive Manufacturing* (Vol. 21, pp. 1–16). Elsevier B.V. <https://doi.org/10.1016/j.addma.2018.01.002>
- [4] Naranjo-Lozada, J., Ahuett-Garza, H., Orta-Castañón, P., Verbeeten, W. M. H., & Sáiz-González, D. (2019). Tensile properties and failure behavior of chopped and continuous carbon fiber composites produced by additive manufacturing. *Additive Manufacturing*, 26, 227–241. <https://doi.org/10.1016/j.addma.2018.12.020>
- [5] Kabir, S. M. F., Mathur, K., & Seyam, A. F. M. (2020). A critical review on 3D printed continuous fiber-reinforced composites: History, mechanism, materials and properties. In *Composite Structures* (Vol. 232). Elsevier Ltd. <https://doi.org/10.1016/j.compstruct.2019.111476>
- [6] van de Werken, N., Tekinalp, H., Khanbolouki, P., Ozcan, S., Williams, A., & Tehrani, M. (2020). Additively manufactured carbon fiber-reinforced composites: State of the art and perspective. In *Additive Manufacturing* (Vol. 31). Elsevier B.V. <https://doi.org/10.1016/j.addma.2019.100962>
- [7] Nawafleh, N., & Celik, E. (2020). Additive manufacturing of short fiber reinforced thermoset composites with unprecedented mechanical performance. *Additive Manufacturing*, 33. <https://doi.org/10.1016/j.addma.2020.101109>

- [8] Lee, K. J., Jeon, M. S., & Lee, J. R. (2023). Evaluation of manufacturing defects in 3D printed carbon fiber reinforced cylindrical composite structure based on laser ultrasonic testing. *NDT and E International*, 135. <https://doi.org/10.1016/j.ndteint.2023.102802>
- [9] Liao, G., Li, Z., Cheng, Y., Xu, D., Zhu, D., Jiang, S., Guo, J., Chen, X., Xu, G., & Zhu, Y. (2018). Properties of oriented carbon fiber/polyamide 12 composite parts fabricated by fused deposition modeling. *Materials and Design*, 139, 283–292. <https://doi.org/10.1016/j.matdes.2017.11.027>
- [10] Gholizadeh, S. (2016). A review of non-destructive testing methods of composite materials. *Procedia Structural Integrity*, 1, 50–57. <https://doi.org/10.1016/j.prostr.2016.02.008>
- [11] Tan, K. T., Watanabe, N., & Iwahori, Y. (2011). X-ray radiography and micro-computed tomography examination of damage characteristics in stitched composites subjected to impact loading. *Composites Part B: Engineering*, 42(4), 874–884. <https://doi.org/10.1016/j.compositesb.2011.01.011>
- [12] Caminero, M. A., García-Moreno, I., Rodríguez, G. P., & Chacón, J. M. (2019). Internal damage evaluation of composite structures using phased array ultrasonic technique: Impact damage assessment in CFRP and 3D printed reinforced composites. *Composites Part B: Engineering*, 165, 131–142. <https://doi.org/10.1016/j.compositesb.2018.11.091>
- [13] Drake, T., Bentouhami, F., Campagne, B., Cuevas, E., Drake, T., Dubois, M., Fraslin, T., Piñeiro, P., Serrano, J., & Voillaume, H. (2010). LUCIE-A flexible and powerful Laser Ultrasonic system for inspection of large CFRP components. <https://www.researchgate.net/publication/236208610>
- [14] Scruby, C. B. (1989). Some applications of laser ultrasound. *Ultrasonics*, 27(4), 195-209.
- [15] Lee, J. R., Ciang Chia, C., Park, C. Y., & Jeong, H. (2012). Laser ultrasonic anomalous wave propagation imaging method with adjacent wave subtraction: Algorithm. *Optics and Laser Technology*, 44(5), 1507–1515. <https://doi.org/10.1016/j.optlastec.2011.12.008>
- [16] Hong, S. C., Abetew, A. D., Lee, J. R., & Ihn, J. B. (2017). Three dimensional evaluation of aluminum plates with wall-thinning by full-field pulse-echo laser ultrasound. *Optics and Lasers in Engineering*, 99, 58–65. <https://doi.org/10.1016/j.optlaseng.2016.08.010>
- [17] Lee, J. R., Jeong, H., Ciang, C. C., Yoon, D. J., & Lee, S. S. (2010). Application of ultrasonic wave propagation imaging method to automatic damage visualization of nuclear power plant pipeline. *Nuclear Engineering and Design*, 240(10), 3513–3520. <https://doi.org/10.1016/j.nucengdes.2010.06.011>
- [18] Lee, J. R., Ciang Chia, C., Park, C. Y., & Jeong, H. (2012). Laser ultrasonic anomalous wave propagation imaging method with adjacent wave subtraction: Algorithm. *Optics and Laser Technology*, 44(5), 1507–1515. <https://doi.org/10.1016/j.optlastec.2011.12.008>